PCCP

Accepted Manuscript

This is an *Accepted Manuscript*, which has been through the Royal Society of Chemistry peer review process and has been accepted for publication.

Accepted Manuscripts are published online shortly after acceptance, before technical editing, formatting and proof reading. Using this free service, authors can make their results available to the community, in citable form, before we publish the edited article. We will replace this *Accepted Manuscript* with the edited and formatted *Advance Article* as soon as it is available.

You can find more information about *Accepted Manuscripts* in the Information for Authors.

Please note that technical editing may introduce minor changes to the text and/or graphics, which may alter content. The journal's standard Terms & Conditions and the Ethical guidelines still apply. In no event shall the Royal Society of Chemistry be held responsible for any errors or omissions in this *Accepted Manuscript* or any consequences arising from the use of any information it contains.

ROYAL SOCIETY OF CHEMISTRY

www.rsc.org/pccp

Metastable alloy nanoparticles, metal-oxide nanocrescents and nanoshells generated by laser ablation in liquid solution: influence of the chemical environment on structure and composition

Stefano Scaramuzza, Stefano Agnoli, Vincenzo Amendola*

Department of Chemical Sciences, Università di Padova, via Marzolo 1, I-35131 Padova, Italy
* correspondence: vincenzo.amendola@unipd.it

Abstract

Alloy nanoparticles are characterized by the combination of multiple interesting properties which are attractive for technological and scientific purposes. A frontier topic of this field is represented by nanoalloys with composition not thermodynamically allowed at ordinary temperature and pressure (i.e. metastable), because they require out-of-equilibrium synthetic approaches. Recently, laser ablation synthesis in solution (LASiS) has been successfully applied to the realization of metastable nanoalloys thanks to the fast kinetics of nanoparticles formation. However, the role played by the chemical environment on the final composition and structure of laser generated nanoalloys still has to be fully elucidated. Here we investigated the influence of different synthetic conditions on the LASiS of metastable nanoalloys composed by Au and Fe, such as the use of water instead of ethanol, the bubbling of inert gases and the addition of few vol% of H_2O_2 and H_2O. The two elements showed different reactivity when LASiS was performed in water instead of ethanol, while minor effects are observed by bubbling pure gases such as N_2, Ar and CO_2 in the liquid solution. Besides, the plasmonic response and the structure of nanoalloys was sensibly modified by adding H_2O_2 to water. We also found that nanoparticles productivity is dramatically influenced just by adding 0.2% of H_2O in ethanol. These results suggest that the formation of a cavitation bubble with long lifetime and large size during LASiS is useful for the preservation of metastable alloy composition, whereas an oxidative environment hamper the formation of metastable alloy nanoparticles. Overall, by acting on the type of solvent and solutes, we were able to switch from a synthetic approach conservative for the compostion of Au-Fe nanoalloys to a reactive environment which gives unconventional structures such as metal@iron-oxide nanoshells and nanocrescents of oxide supported on metal nanospheres. These results expand the knowledge about the mechanism of formation of nanoalloys by LASiS, and show how to obtain multielement nanoparticles of huge interest for nanomedicine, plasmonics, magneto-plasmonics and catalysis.

Physical Chemistry Chemical Physics Accepted Manuscript

Introduction

The field of alloy nanoparticles (NPs) is in rapid expansion due to the large number of possible applications such as in catalysis,[1, 2] sensing,[3] energy storage and conversion,[4] and nanomedicine.[5-7] In fact, multiple properties are brought by the distinct elements composing the alloy, which are interesting also for the investigation of new photonic, magnetic, plasmonic and chemical phenomena.[8] At the same time, the use of computational methods for the prediction of structure and physical-chemical properties of nanoalloys has grown exponentially in recent years.[9-12]

A special position in this panorama is occupied by nanoalloys with composition not thermodynamically allowed at ordinary temperature and pressure (i.e. metastable). The synthesis of metastable nanoalloys is challenging and requires out-of-equilibrium synthetic approaches, which usually relies on very short NPs formation time.[8, 13] The preparation of metastable alloys composed by elements with similar lattice parameters, electronic configuration and chemical reactivity is sometimes possible by wet chemistry methods. For instance PdAu and PtAu nanoalloys have been produced and investigated for catalytic applications.[14, 15] In the most critical cases, where electronic structure and different reactivity of the elemental constituents in the alloy prevents the use of traditional synthetic approaches, nanoalloys can be obtained by physical methods, such as spark discharge,[16] inert gas condensation within sputtering chambers,[17] vacuum co-evaporation,[18] laser sputtering in vacuum[19] or, in liquid phase, by radiolysis of chemical precursors.[20-22]

The payback of out-of-equilibrium synthetic efforts is high, because it consists in the realization of NPs with unprecedented composition, structure, properties and applications, which can not be found simply by building composite nanostructures like core@shell, core@satellite or dumbbells NPs.[8, 13]

Recently, laser ablation synthesis in solution (LASiS) has been successfully applied to the realization of metastable nanoalloys thanks to the fast kinetics of nanoparticles formation.[23, 24] In LASiS, NPs are generated as a colloidal solution by ablation of a bulk material dipped in a liquid solution.[23, 25] This technique gives the access to a wide library of NPs just by varying the composition of the bulk target and of the liquid solution.[23] LASiS avoids most typical problems of chemical synthesis, such as the use and disposal of environmentally unfriendly, toxic or costly reagents.[23, 25] In addition, LASiS has a simple experimental set up which requires only limited manual operation, can be performed in continuous flow and requires raw materials such as bulk targets and common solvents, maintaining low the production costs.[23, 25] Another important advantage is the possibility to conjugate nanoparticles with polymers, biomolecules or other organic moieties in one step.[23, 25]

The chemical environment during LASiS plays a crucial role on the formation of NPs, although this is still an open topic with several unclear points.[23] Indeed, only few reports considered the effect of

Physical Chemistry Chemical Physics Accepted Manuscript

the synthetic environment on the LASiS of nanoalloys. For instance, different effects on the composition of NiFe and SmCo alloy NPs were observed during LASiS in cyclopentanone.[26] Morphological differences in Ag-Cu alloys were also reported as a function of the composition of the bulk target used for LASiS in water.[27] In addition, the modification of the solvent was used to tune the composition of metastable Au-Fe nanoalloys.[28] In other experiments, core@shell structures with minimal interfacial alloying were obtained by laser ablation of Ag in a reactive environment containing Pd(II) ions,[29] or elongated alloy structures were produced by LASiS in superfluid He.[30] Therefore, the control of LASiS chemical environment is crucial to disclose a wide library of nanoalloys and to improve the control over the structure of already achievable alloy NPs.

Here we investigated the influence of different synthetic conditions on the LASiS of metastable nanoalloys composed by Au and Fe. These two elements represent an useful case-study because show different reactivity in oxidising environments, and the Au-Fe alloys with Fe content exceeding ca. 3% are not thermodynamically stable at room temperature and pressure.[31] Therefore, we tested how the products are influenced by the presence of oxidants such as H_2O_2 or by bubbling pure gases such as N_2, Ar and CO_2 in the liquid solution. The experiments considered the two opposite cases of an oxidising liquid such as water and of a less oxidising, i.e. "conservative", liquid such as ethanol. We observed that the synthetic environment influenced several features of the NPs, ranging from the size distribution to the plasmonic response, the surface structure and even the productivity of nanoalloys. In particular, by acting on the type of solvent and solutes, we show how to switch from a conservative synthetic procedure for the composition of metastable Au-Fe nanoalloys to the preparation of more complex structures such as core@shell metal@iron-oxide nanoparticles. Overall, this study evidenced the importance of chemical interactions between solution species and ablated materials, as well as the influence of solution decomposition on the rise of the cavitation bubble, which affects the coalescence and growth of nanoparticles.

On the one hand, these results contribute to expand the knowledge about the mechanism of formation of nanoalloys by LASiS, and are helpful for the control and the predetermination of products. On the other hand, the synthesis of bimetallic Au-Fe nanoalloys is very important to achieve both plasmonic and magnetic properties in the same NPs, and our results show how to obtain multielement nanoparticles of huge interest for nanomedicine, plasmonics, magneto-plasmonics and catalysis.

Experimental methods.

LASiS was performed with 6 ns (50 Hz) laser pulses at 1064 nm and 65 mJ/pulse focused with a f:150mm lens on a glass cell containing a bulk $Au_{73}Fe_{27}$ alloy plate (99.9% pure, from Mateck)

Physical Chemistry Chemical Physics Accepted Manuscript

dipped in 4 mL of liquid solution.[24, 28] Each synthesis lasted for 30', after which the NPs colloidal solutions were mixed with an equal amount of water containing 4 mg/mL of disodium ethylenediaminetetraacetic acid (EDTA, form Sigma-Aldrich) and >0.01 mg/mL of thiolated poly(ethylene glycol) methyl ether (PEG, 5000 Da from Laysan Bio) and heated at 60 °C for 1 hour, according to our previously established procedure.[24, 28, 32] Then, the NPs solutions were dialysed with concentration tubes with a cut-off weight of 10000 Da (Sartorius). After multiple washing cycles, NPs were recollected in distilled water.

For LASiS, either distilled water or HPLC grade ethanol (from Sigma-Aldrich) were used. Solvents were used as received or after bubbling different gases. Bubbling was performed at 1.1 atm of gas pressure for 30' in 50 mL flasks filled with solvent brought to the boiling, followed by additional 30' to reach equilibrium with room temperature after boiling. Then, the liquid was immediately used for LASiS.

LASiS was performed also in H_2O or ethanol containing 0.3% in volume of H_2O_2 (35vol% in water, from Merck), and in ethanol containing 0.2% in volume of distilled water.

UV-Visibile absorption spectra were acquired with an Agilent Cary 5000 spectrometer using 2 mm optical path quartz cells.

Transmission electron microscopy (TEM) analysis was performed with a FEI Tecnai G2 12 operating at 100 kV and equipped with a TVIPS CCD camera. Samples were prepared by drop casting on copper grids coated with amorphous carbon films.

XPS analysis was performed at room temperature using normal emission geometry with a modified VG ESCALAB MKII (Vacuum generators, Hastings, England) equipped with a twin (Mg/Al) anode X-ray source, a sputter gun, and a hemispherical electrostatic analyzer with a five channel detector. We used the Al-Kα radiation (1486.6 eV) as an excitation source.

Samples for the XPS analysis were synthesized by the same procedure described above, but without the addition of PEG, in order to avoid shielding of the NPs surface.

The sample composition has been determined by using the theoretical photoionisation cross sections by Yeh and Lindau[33] and the electron inelastic mean free path calculated using the TPP-2 formula.[34]

Modelling of the optical properties was performed according to previously published protocols which exploit the Mie model for compact spheres[24, 28, 35, 36] and its extension for core-shell spheres.[35, 37, 38] These models were used to fit the experimental UV-vis absorption spectrum in the 300-600nm interval. As input data, we used the histogram of sizes measured by TEM analysis, while we used the alloy composition as fitting parameter. In case of the Mie model for core-shell spheres, the shell thickness was also used as the second fitting parameter. The optical constants of the Au-Fe alloy were obtained according to the procedure described in ref.[24, 28] and corrected for size effects as

Physical Chemistry Chemical Physics Accepted Manuscript

described in previously.[24, 36] Optical constants for AuFe alloy were taken from ref.[39], and for Au and iron oxide (magnetite Fe_3O_4) from ref.[40]. For the surrounding matrix we used the refractive index of the solvent (n=1.334).

Results

The UV-visible spectra of NPs generated by laser ablation in water solutions are reported in Figure 1a. In all cases, a sharp absorption band at visible frequencies is observed, originated by the surface plasmon resonance (SPR) of Au-Fe nanoalloys, together with an absorption edge in the near UV region, originated by single electron interband transitions in metallic Au-Fe solid solutions.[24, 28, 39] The SPR is a clear indication that nanometric particles are formed,[24, 28] and its position in proximity of 520 nm is compatible with spherical particles,[25, 36] in agreement with what is usually observed during LASiS of noble metal NPs.[25]

In case of water solution (black line in Figure 1a), the intensity and the shape of the SPR band is compatible with gold-rich alloy NPs, according to what reported recently for AuFe NPs containing only about 3at% of Fe.[28] The results obtained in H_2O treated with N_2, Ar and CO_2 are very similar to the reference H_2O solution, suggesting that in all these cases the majority of Fe is lost during LASiS. Only in case of the sample obtained in water/CO_2, we observe a slightly larger absorbance in the red spectral region, which is compatible with the presence of aggregates of NPs.[7, 36]

By laser ablation in presence of the oxidant H_2O_2 molecules, instead, a remarkable red shift up to a wavelength of 560 nm and broadening of the SPR are observed. Such a red shift in Au-based nanostructure is compatible with the existence of metal nanospheres surrounded by a dielectric shell with refractive index larger than the solvent matrix, i.e. a core@shell metal@dielectric structure.[37, 38, 41] To further substantiate the hypothesis about the formation of nanoshells, we performed TEM analysis on these NPs. As shown in Figure 1b, NPs are prevalently composed by an inner region with high electronic contrast, which appears dark in the TEM image and is indicative of a metal lattice rich of Au atoms, and an outer shell with lower electronic contrast, which appears grey and is indicative of a non-metallic phase with low-Z elements such as iron oxide. The size distribution, reported in Figure 1c, is bimodal and can be described with two gaussian cruves centred respectively at 6 ± 1 nm and 24 ± 13 nm. This is a remarkable difference with the monomodal lognormal size distribution usually observed in NPs obtained by LASiS with ns laser pulses, and it is a clear indication of the occurrence of two distinct synthetic environments during the formation of NPs.[23, 25] We also observed the presence of several NPs with intermediate size (of the order of 10nm) with elongated and irregular corral-like structure, while smaller and bigger particles have a more regular spherical shape.

Physical Chemistry Chemical Physics Accepted Manuscript

The UV-vis absorption spectrum of the water/H_2O_2 sample was fitted with the Mie model for a spherical nanoshell with metal core surrounded by a dielectric shell of iron oxide (Figure 1d). In this fitting model, the nanoshell is isolated in a water matrix and the experimentally measured size histogram is provided as input data, while the composition of the alloy and the thickness of the dielectric shell are used as fitting parameters. Modelling the optical properties of Au-Fe NPs with the Mie model is a reliable way to obtain information about the alloy composition, because the SPR is directly influenced by the electronic band structure of gold alloyed with iron.[24, 28, 39] Conversely, several other investigation techniques are sensible only to the elemental abundance of iron and gold in the NPs, but cannot discriminate between iron oxide and metal iron actually included in the alloy. Besides, by using the experimentally measured size histogram as input data for Mie modelling, we account for all the NPs in the samples, weighted for their abundance and volume.

In the present case, the best agreement between fit and experiment was found for an alloy composition of Au 96at% and Fe 4at% and a shell thick 0.125 times the radius of the metal core (red line in Figure 1d). This composition is close to that previously reported for AuFe nanoalloys obtained by LASiS in aqueous environment.[28] We noticed that the experimental spectrum is not well fitted in the red and near infrared range, where corral like and aggregated NPs contribute to the optical density of the sample, in fact these shapes are not accounted by the Mie model for isolated spherical nanoshells.[35]

Importantly, when the same fitting procedure is performed with a core of pure Au, i.e. limiting the parameters to the thickness of the shell only, the fitting result is far from the experiment (green line in Figure 1d), due to the superior intensity of the SPR compared to interband transitions at short wavelengths. We also performed the fit of the experimental spectrum with the Mie model for simple spheres (i.e. not nanoshells), by considering the alloy composition as the fitting parameter, and we found that the model fails in predicting the exact position of the SPR, further confirming that the oxide shell is responsible for the red shift of the plasmon band.

Physical Chemistry Chemical Physics Accepted Manuscript

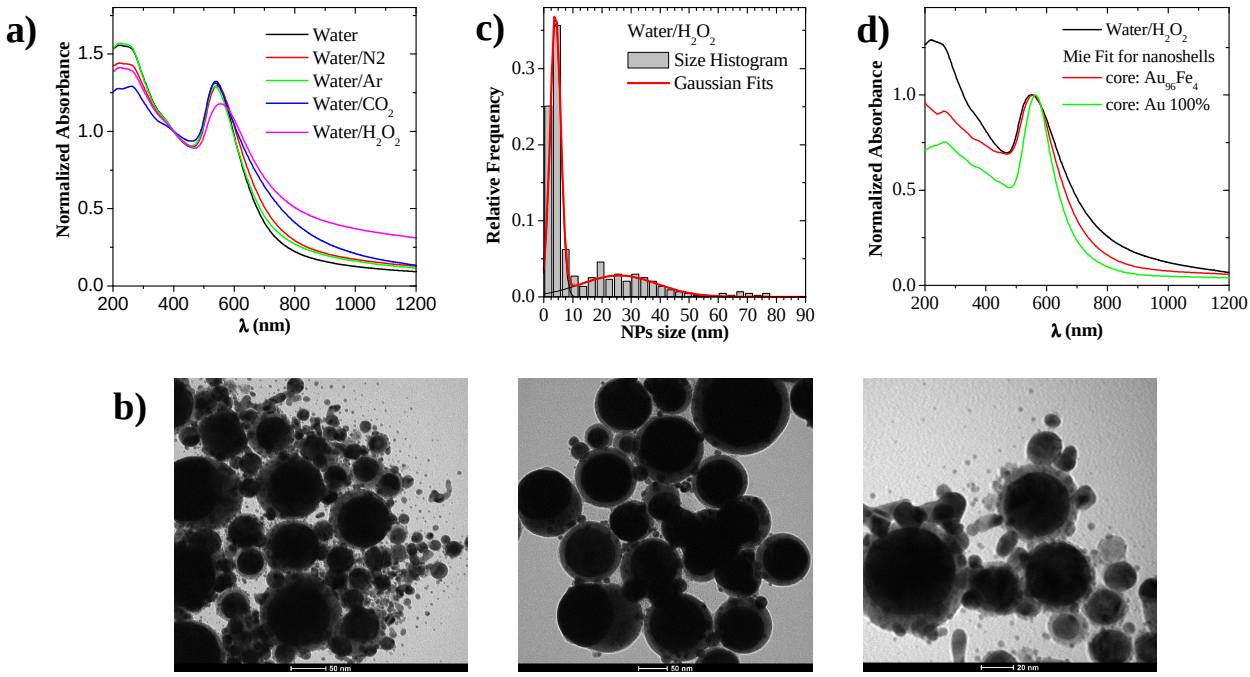

Figure 1. a) UV-Visible spectra of the AuFe NPs obtained in water solutions. All spectra were normalized at 400 nm for ease of comparison. b) Representative TEM images of NPs in the water/H_2O_2 sample, where the oxide shell surrounding the metal core is clearly visible. c) Size histogram of NPs in the water/H_2O_2 sample. The size distribution is bimodal and was fitted with two gaussian curves. d) Mie fit of the experimental UV-vis spectrum of the water/H_2O_2 sample. All spectra are normalized at the SPR maximum for ease of comparison.

The UV-visible spectra of NPs generated by laser ablation in ethanol solutions are reported in Figure 2a. The reference solution obtained in ethanol is characterized by the presence of an SPR band much damped compared to those of NPs obtained in water solutions. This is in agreement with what expected for the LASiS of AuFe NPs in pure ethanol,[24, 28] and it is a clear indication of the formation of nanoalloys with iron content of the order of 10-13%, according to what previously observed.[24, 28] The damping of the SPR is observed also for NPs obtained in ethanol treated with N_2, Ar and CO_2, suggesting that synthesis results are similar. From the TEM analysis performed on the sample obtained in ethanol/N_2 (Figure 2b), we observed that NPs are spherical and do not have any shell with lower electronic contrast, contrary to the particles shown in Figure 1b. More in detail we observed that some of the small (<10nm) NPs have irregular corals-like shape, while larger NPs all have a well defined spherical shape. The size distribution (reported in Figure 2c) is monomodal with average NPs size of 19 ± 14 nm and lognormal profile, in agreement with what usually found during LASiS of metal NPs.

The UV-vis absorption spectrum of the ethanol/N_2 sample was fitted with the Mie model for isolated spherical NPs in a water matrix (figure 2d), using the composition of the alloy as fitting parameter and the experimentally measured size histogram as input data. The best agreement was

Physical Chemistry Chemical Physics Accepted Manuscript

found for an alloy composition of Au 90at% and Fe 10at%, as expected on the basis of previous laser ablation synthesis in similar environment.[24, 28] Also in this case, the experimental spectrum is not well fitted in the red and near infrared region, where the plasmon absorption of nonspherical and aggregated NPs are located. The optical properties of pure Au NPs with the same size distribution found experimentally is also reported in Figure 2d for comparison (green line), in order to show that the SPR is much more intense in pure Au NPs with same size.

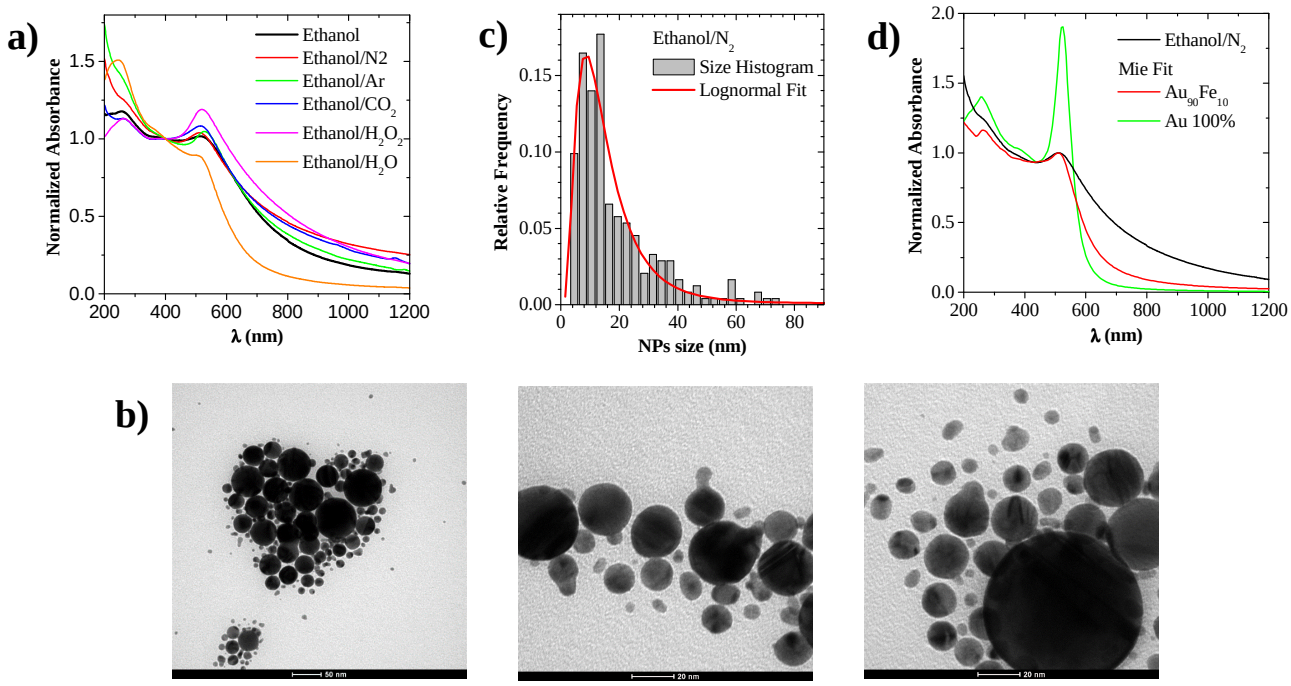

Figure 2. a) UV-Visible spectra of the AuFe NPs obtained in ethanol solutions. All spectra were normalized at 400 nm for ease of comparison. b) Representative TEM images of NPs in the ethanol/N_2 sample. c) Size histogram of NPs in the ethanol/N_2 sample. The size distribution is monomodal and was fitted with a lognormal curve. d) Mie fit of the experimental UV-vis spectrum of the ethanol/N_2 sample. All spectra are normalized at 400 nm for ease of comparison.

Also in the ethanol/H_2O_2 sample, the damping and the position of the SPR is compatible with the formation of alloy NPs. Interestingly, there is no evidence of red shift like that observed after LASiS in water/H_2O_2 solution. Therefore, the optical absorption spectrum suggests that a nanometric oxide shell is not present around NPs. This is confirmed by TEM analysis (Figure 3a), which instead showed the presence of spherical NPs with regular shape and morphology similar to the products obtained in ethanol/N_2 environment. The size distribution is lognormal (Figure 3b), with average size of 38 ± 19 nm, corresponding to twice the value found for the sample obtained in ethanol/N_2.

The Mie fitting of the UV-vis absorption spectrum of the ethanol/H_2O_2 sample is reported in Figure 3c. Similar to the ethanol/N_2 sample, also in this case the best agreement was found for an alloy

Physical Chemistry Chemical Physics Accepted Manuscript

composition of Au 90at% and Fe 10at% (red line in Figure 3c). This means that the larger SPR intensity is due to the larger size of NPs obtained in ethanol/H_2O_2. Again, the experimental spectrum is not well fitted in the red and near infrared region, likely due to the presence of nonspherical and aggregated NPs. The difference with the optical properties of pure Au NPs with the same size (green line in Figure 3c) is remarkable, as in the ethanol/N_2 case, further confirming that our sample contains Au-Fe alloy NPs.

The H_2O_2 solution added to ethanol is 35% in volume, hence it contains two parts of H_2O for each part of H_2O_2. In order to obtain more insights about the distinct role of H_2O and H_2O_2, we also performed the synthesis in ethanol containing only 0.2% of distilled water. Interestingly, we found remarkable differences compared to the ethanol/H_2O_2 case for what concerns both the SPR and the NPs morphology. Regarding the SPR (orange line in Figure 2a), we observed a damping comparable to the reference ethanol solution, which is indicative of the formation of alloy NPs. On the other hand, the absorption band due to interband transitions is more intense than in the other samples (all the spectra are normalized at 400nm for simplicity of comparison), and this can be due to the presence of a large number of particles which are too small to show appreciable SPR absorption. In fact, the absorption tail in the red and near infrared region is lower than in the other samples, which is again compatible with small NPs with negligible scattering cross section. TEM analysis supported the information extracted from UV-visible spectroscopy, showing that the sample is composed by a multitude of small (<5 nm) NPs and by a minority of larger nanospheres with size of tens of nm (Figure 3d). Importantly, most of the large nanospheres are characterized by an iron oxide crescent with low electronic contrast on one side, which confers an asymmetric structure to the NPs. The thickness of the nanocrescent is of 1 - 4 nm and it is reminiscent of the iron oxide shell of the sample obtained in water/H_2O_2 solution (Figure 1b), although asymmetric and with smaller thickness. The size distribution (Figure 3e) is constituted by a sharp peak at 4 nm followed by a plateaux in the 10 - 40 nm region, and can be modelled with two gaussian profiles centred respectively at 4 ± 4 nm and 20 ± 21 nm. This type of size distribution is different from the previous cases of ethanol/N_2 and ethanol/H_2O_2, while it has again some similarities with the NPs obtained in water/H_2O_2.

The UV-vis absorption spectrum of the ethanol/H_2O sample was fitted with both the Mie model for simple spheres and spherical nanoshells (Figure 3f), in fact the NPs are half way between these two simplified structures. Indeed, the results are similar, since the best agreement was found for Au89at% - Fe11at% and Au 88at% - Fe 12at% using, respectively, the simple sphere model (red line in Figure 3f) or the nanoshell model (with a shell thick 0.05 times the radius of the metal core, blue line in Figure 1d). The composition is close to that obtained for the ethanol/N_2 and

Physical Chemistry Chemical Physics Accepted Manuscript

ethanol/H_2O_2 samples. Therefore, metal NPs in the ethanol/H_2O sample are composed by Au-Fe alloy, although they are partially coated by iron oxide nanocrescents. The quality of the fit in the red and near infrared range is superior to all the previous cases, suggesting that the number of nonspherical or aggregated NPs is negligible. A further confirmation of the formation of AuFe alloy is obtained by performing the fitting procedure with the optical constant of pure Au, since the best result achievable is very far from the experiment, due to the much larger intensity of the SPR (green and orange lines in Figure 1d for, respectively, simple spheres and nanoshells).

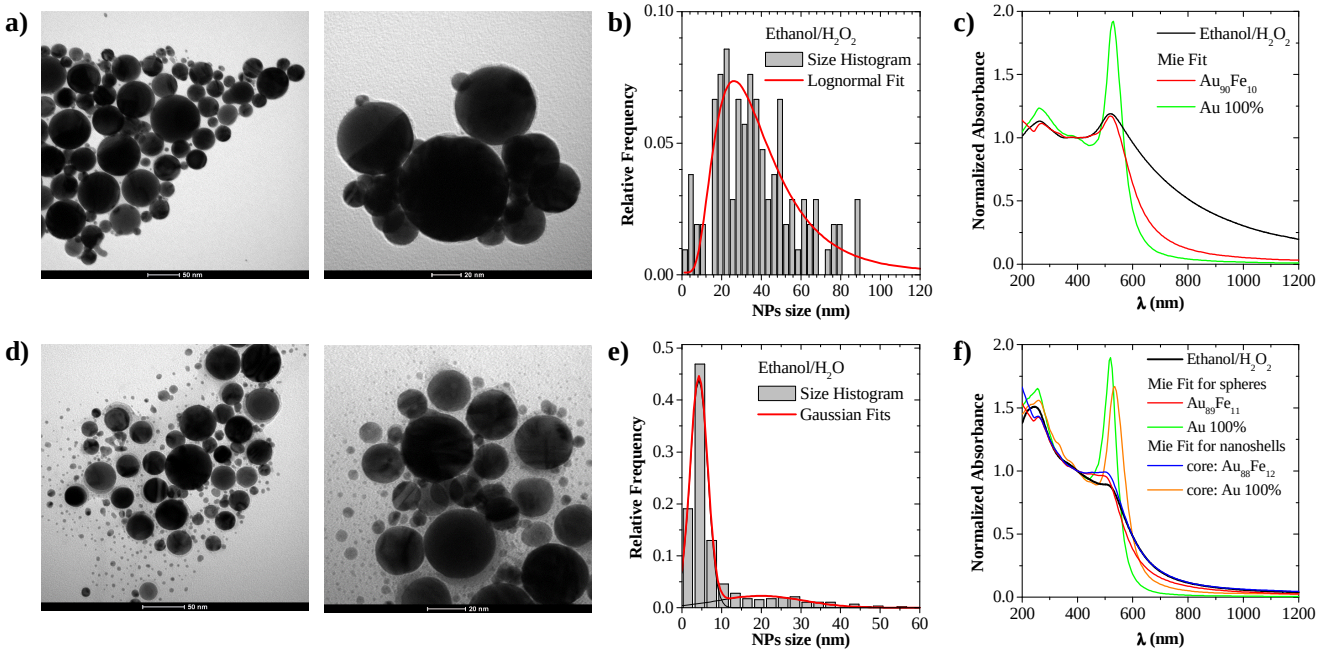

Figure 3. a) Representative TEM images of NPs in the ethanol/H2O2 sample. b) Size histogram of NPs in the ethanol/H2O2 sample. The size distribution is monomodal and was fitted with a lognormal curve. c) Mie fit of the experimental UV-vis spectrum of the ethanol/H2O2 sample. All spectra are normalized at 400 nm for ease of comparison. d) Representative TEM images of NPs in the ethanol/H2O sample. Oxide nanocrescents are observed in larger nanoparticles e) Size histogram of NPs in the ethanol/H2O sample. The size distribution is bimodal and was fitted with two gaussian curves. f) Mie fit of the experimental UV-vis spectrum of the ethanol/H2O sample. The fit was performed with both the models for simple spheres and metal@oxide nanoshells. All spectra are normalized at 400 nm for ease of comparison.

According to TEM analysis, iron oxidation is more evident by LASiS in ethanol/H_2O than in ethanol/H_2O_2, which instead gives results comparable to ethanol/N_2. To further asses this finding, we investigated the surface chemical nature of NPs by XPS. In all cases, we found an Au 4f doublet located at the binding energy (BE) expected for metal NPs (Figure 4a), and the peaks of C 1s are

Physical Chemistry Chemical Physics Accepted Manuscript

located at the BE proper of adventitious carbon (Figure 4b), while there are no signals compatible with the presence of iron carbide, in agreement with what recently reported for these nanosystems.[28] The Fe 2p signal (Figure 4c) is also similar in the three samples and composed by multiple contributions which span the BE range proper of metal iron (707-707.5 eV), iron(II) oxide (709.5 eV) and iron(III) oxide (711 eV). The presence of the shoulder at BE of Fe(0) in all the three samples is even more evident by comparison with the Fe 2p spectrum collected on a reference of magnetite (black circles in Figure 4b). Therefore, the surface of the AuFe NPs is passivated by the presence of metal Au and iron oxide, protecting from further oxidation the metal iron inside the nanoparticle. This is in agreement with previous findings about AuFe NPs and explains the excellent stability in water and air for indefinite time of the nanoalloys.[28]

Interestingly, we observed that the spectra collected on the ethanol/N_2 and ethanol/H_2O_2 samples are well superimposable, while the peak of the ethanol/H_2O sample shows a slightly larger iron oxide component. However, the main difference evidenced by XPS among the three samples consists in the Fe/Au atomic ratio on the surface of NPs, which is of 20/80, 20/80 and 30/70 for the samples obtained, respectively, in ethanol/N_2, ethanol/H_2O_2 and ethanol/H_2O. This is a further indication that iron oxidation and segregation on NPs surface occurred in samples obtained in the presence of H_2O, as well as that the chemical nature of NPs surface in ethanol/N_2 and ethanol/H_2O_2 samples is very similar.

Overall, XPS results confirmed the previous observation about structural analogies between ethanol/N_2 and ethanol/H_2O_2 samples, as well as the larger surface oxidation in the ethanol/H_2O sample.

Physical Chemistry Chemical Physics Accepted Manuscript

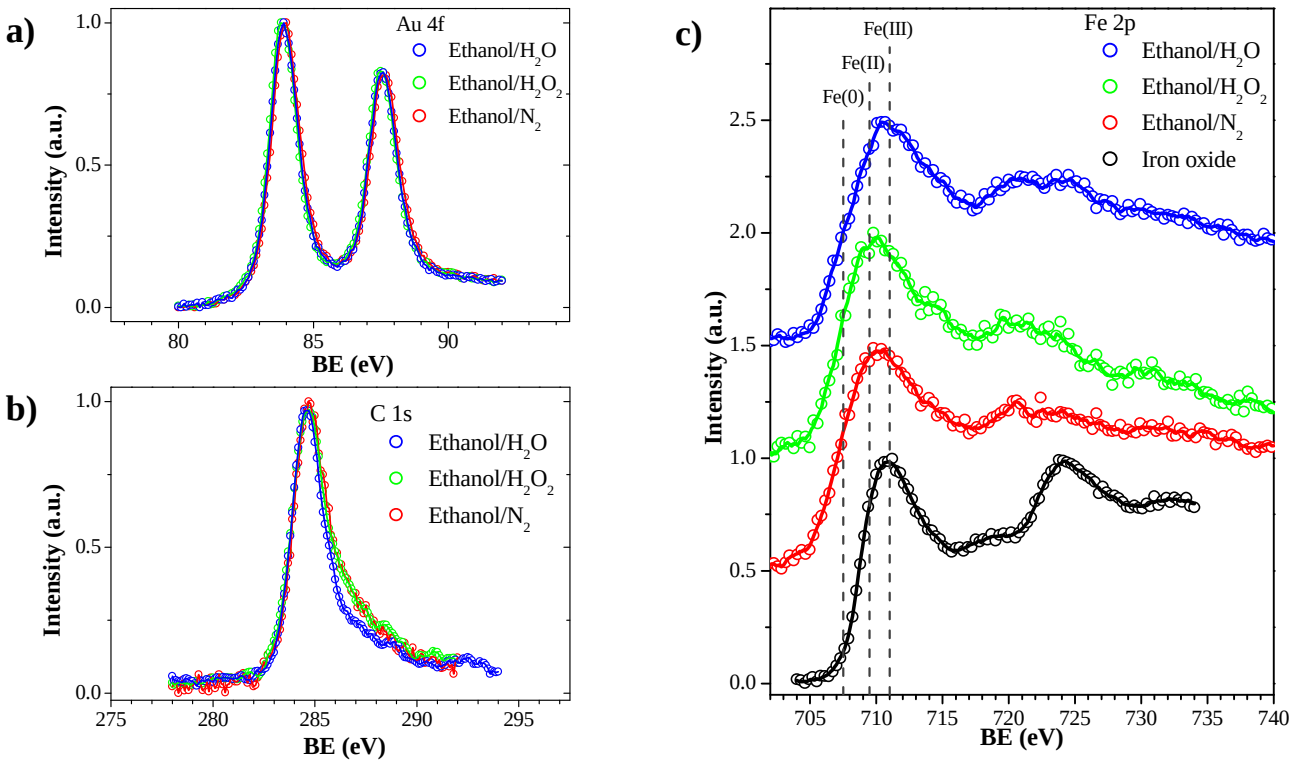

Figure 4. a) Au 4f doublet. b) C 1s peak. c) Fe 2p peak. The spectrum collected on a iron oxide (magnetite) sample is also shown for comparison (black circles). All spectra are vertically shifted for clarity. Dashed lines show the BE of Fe(0), Fe(II) and Fe(III).

The experiment performed in ethanol/H_2O is characterized also by a remarkably high NPs productivity compared to all the other ethanol and water solutions. In Figure 5 we reported the productivity for the different solutions at parity of all the other synthesis conditions, expressed in μg/pulse. Although the productivity in water solution fluctuates around 0.0035 μg/pulse, i.e. 1.75 times larger than in ethanol, the addition of 0.2vol% of water to ethanol boosted the productivity to 0.008 μg/pulse, i.e. 2.3 times the water value. The same result is not obtained by the addition of 0.3vol% of H_2O_2 (35vol% solution in water).

Physical Chemistry Chemical Physics Accepted Manuscript

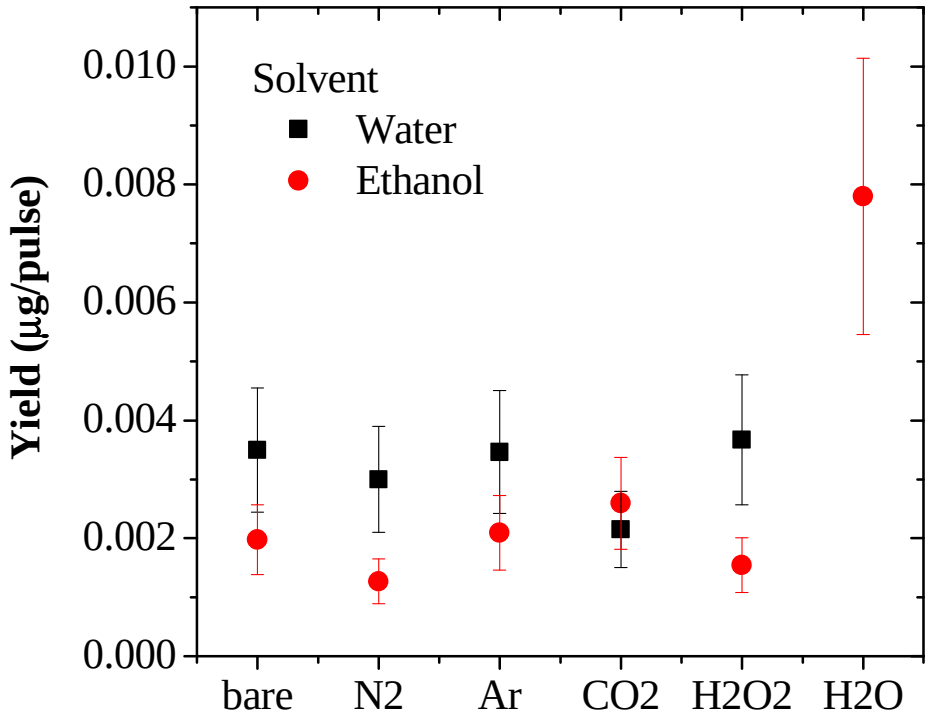

Figure 5. Productivity of metal NPs (expressed in µg/pulse) in the different solution studied in this work. Black circles: water solutions; red circles: ethanol solutions.

In summary, the experiments about LASiS in different chemical environments showed the following main results:

i) Water induces the formation of heterostructures composed by metal cores and iron oxide shells or crescents, together with a large majority (in number) of small metal NPs (i.e. with bimodal size distribution). Consequently, the quantity of Fe in the AuFe alloy is reduced compared to ethanol. However the same effect is not observed in ethanol/H_2O_2 environment.

ii) Ethanol induces the formation of AuFe alloys with monomodal (lognormal) size distribution, and with average size and iron content larger than in water.

iii) NPs productivity is enhanced by the addition of 0.2vol% of H_2O to ethanol. However, the same effect is not obtained by using H_2O_2 (35vol% in water) instead of pure H_2O.

Discussion.

The control of nanoalloy composition and structure during LASiS is crucial to achieve metastable phases, as well as for the design of multifunctional nanoparticles with optimal size and composition for specific applications in nanomedicine, magneto-plasmonics, sensing or catalysis.

The experimental set up of LASiS is relatively simple and allows the investigation of the role played by the chemical environment on the structure and composition of NPs by maintaining unchanged all the other synthesis parameters. In this study, laser ablation was performed in two solvents which have opposite effects on the composition of Au-Fe nanoalloys. In fact, according to what recently reported,[24, 28] “iron-rich” NPs (about 10-13at% Fe) are obtained in ethanol, while

Physical Chemistry Chemical Physics Accepted Manuscript

"iron-poor" NPs (about 3at% Fe) are obtained in water, even by maintaining unchanged all the other synthesis parameters.

We investigated also the effect of bubbling with inert gases or adding oxidant species such as H_2O_2 to the LASiS of alloy NPs. Bubbling with inert gases is useful to investigate the role of solvent molecules separately from that of the dissolved atmospheric gases in equilibrium with the liquid, such as O_2 or CO_2.[23] For instance, the oxidation of iron can occur by reaction with O_2 molecules as well as with solvent molecules.[23, 24, 28, 42] The Henry constants of O_2 in water and ethanol at 298 K are, respectively, 4.26E+4 atm and 0.17E+4 atm[43, 44] and, since a larger value means lower solubility of the gas, the room pressure and temperature concentration of O_2 in ethanol is larger than in water.[43-45] This is already an indication that the oxidation of Fe in water solution is due to the interaction with solvent molecules, with minimal influence from atmospheric oxygen. This was confirmed by our experiments, since similar products were obtained in water, water/N_2, water/Ar and water/CO_2. In both solvents (ethanol and water), the Henry constants of Ar, N_2 and O_2 are comparable, while CO_2 values are one order of magnitude larger.[43-47] In particular, the solubility in water is of the order of 0.002%-0.006% in weight for Ar, N_2 and O_2 and of 0.2% for CO_2, while it is about 10 times larger in ethanol.[43-47] However, we found minimal or null effects on products by changing the type of gas in equilibrium with the liquid. Therefore, our experiments suggest that the concentration of O_2 and other gases in the solvents used for LASiS play a secondary role compared to solvent molecules, and that CO_2 molecules do not react in a appreciable way with the Au and Fe atoms. In case of CO_2, we only observed an increase of the SPR absorption in the red spectral range, which is compatible with the aggregation of NPs. Indeed, it is known from literature that CO_2 can lower the pH of the solution by reacting with H_2O molecules and forming carbonic acid,[48, 49] which interferes with the colloidal stability of metal NPs obtained by LASiS and promotes particles aggregation.

The predominance of chemical interaction between the ablated material and reactive species at relatively large concentration was further evidenced by adding oxidant solutes such as H_2O_2, at concentration of 0.1vol%, or by adding 0.2vol% H_2O to ethanol. Even a conceptually simple experiment like this originated different results, whose interpretation can be attempted by invoking the dynamics of LASiS.

The following main stages can be identified in LASiS:[23] i) the absorption of the laser pulse by the bulk target (timescale from 0 to 10^{-8} s, i.e. the pulse duration); ii) formation of a plasma plume containing the ablated material, which expands into the surrounding liquid, accompanied by the emission of a shockwave (timescale from 10^{-12} to ca. 10^{-7} s); iii) cooling of the plasma plume and

Physical Chemistry Chemical Physics Accepted Manuscript

release of its energy to the liquid solution, with generation of a cavitation bubble which expands in the liquid and then collapses, by emission of a second shockwave (timescale from 10^{-6} to 10^{-4} s).

The formation of NPs, which is believed to take place by nucleation, nuclei growth and nuclei coalescence, occurs between stages ii) and iii).[23] Instead, only minor processes of slow growth and, eventually, agglomeration and chemical reactions at room temperature occurs after stage iii).

The achievement of AuFe metastable nanoalloys at room temperature and pressure is possible only by the fast cooling rate in stages ii) and iii), otherwise the thermodynamically stable phases would prevail (i.e. pure gold and pure iron, or iron oxide in oxidising environments).[24, 28]

On the other hand, it is important to point out that, when NPs formation occurs in stages ii) and iii), there are 4 main gradients in time and space associated to the 4 parameters which primarily determine the phase and structure of NPs (Figure 6):[23] temperature (T), pressure (p), concentration of the ablated material (C_M) and concentration of solution species (C_S). In fact, due to the hemispherical symmetry of the laser ablation phenomena, the gradients of these 4 parameters are not uniform in space neither constant in time: while T, p and C_M increase by approaching the laser spot on the bulk target, C_S decreases. In addition, the formation of a cavitation bubble induces a spatial discontinuity in the gradients of these 4 parameters and may originate non monotonic spatio-temporal profiles.

Physical Chemistry Chemical Physics Accepted Manuscript

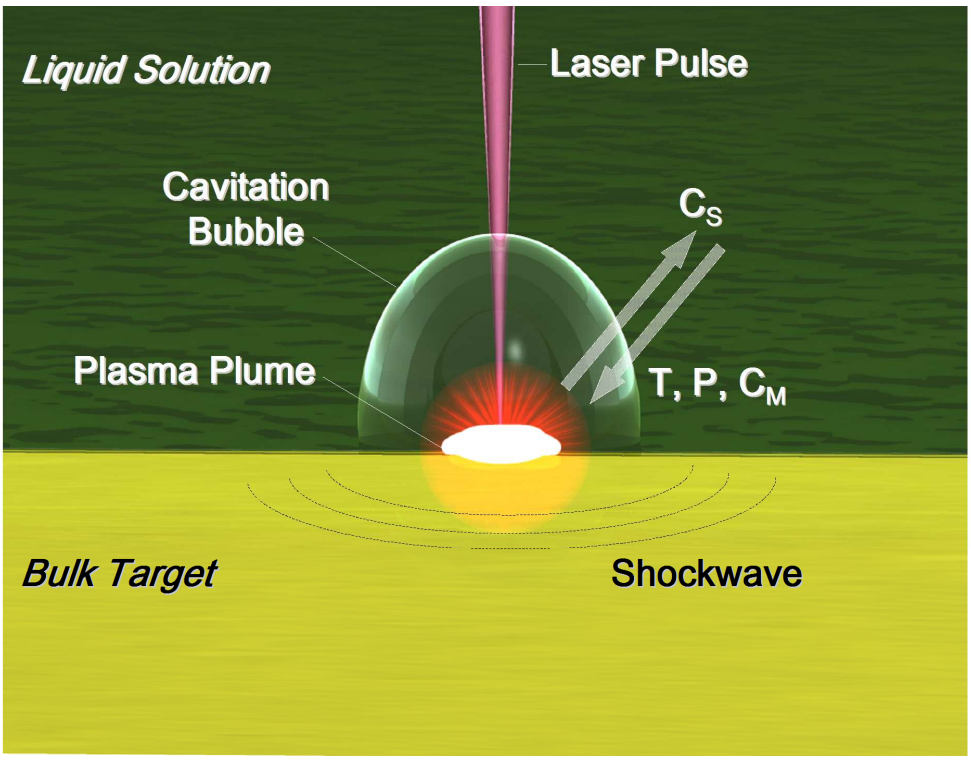

Figure 6. Sketch of the main phenomena involved in LASiS: after absorption of the laser pulse, a plasma is generated above the bulk target, which releases heat to the surrounding liquid promoting the rise of a cavitation bubble. Absorption of the laser pulse also generate a shockwave propagating in two opposite directions. Four main parameters can be identified, whose gradients are rapidly varying in time and space: temperature (T), pressure (p), concentration of target species (C_M) and concentration of solution species (C_S). From ref.23.

Recently, small angle x-ray scattering was used to perform seminal investigations about the localization of NPs in the surrounding of the cavitation bubble.[50, 51] The results showed that only part of the NPs are located inside the cavitation bubble, i.e. in the gas phase, whereas part of the NPs travels with the expanding front of the bubble and, hence, are surrounded by a liquid environment.[50, 51] This observation is crucial to understand the mechanism of formation of NPs because: i) C_M inside the bubble is larger than C_S, i.e. chemical reactions with solution species are more probable outside the bubble; ii) the heat transfer rate in gas is lower than in liquid, i.e. cooling of NPs is more rapid outside the bubble and NPs growth ends earlier.

In particular for the metastable AuFe nanoalloys, where iron atoms are prone to oxidation, the formation of the bimetallic phase is possible only by limiting the probability of reaction with oxidising species. At the same time, XPS measurements showed that surface iron atoms are oxidised, forming a mixed passivating layer of metal Au and iron oxide which protects the metallic interior of the particle at room temperature also in oxidising environments such as in pure water. Numerical calculations showed that, at the nanoscale, the surface has a relevant stabilizing effect on metastable phases,[52, 53] thus it is likely that surface passivation helps in the stabilization of the inner

Physical Chemistry Chemical Physics Accepted Manuscript

AuFe metal alloy. However, if the temperature (i.e. the atomic mobility) of NPs is large, surface oxidation does not produce an efficient passivating effect, and the metal phase is impoverished in the most oxidizable element, which can migrate to the surface and there remains after oxidation. Hence, a crucial role on the final composition and structure of AuFe alloy NPs is played by particles temperature when they pass from the gas/plasma environment to the most oxidising liquid environment.

Based on the above discussion, our experiments in different chemical environments can be classified in four synthetic conditions progressively variable from the most conservative to the most hostile for the formation of the AuFe metastable nanoalloys:

1) Ethanol/H_2O_2 (Figure 7a-b). During LASiS, temperatures of the order of 10^3 K are generated in the ablation site, well above the threshold for H_2O_2 thermal decomposition.[54] Therefore, H_2O_2 decomposition into H_2O and O_2 is possible in the hot area around the ablation site, generating an extra vapor pressure to be summed with that already produced by solvent heating.

The physics of cavitation bubbles is described by the Rayleigh-Plesset equation, which is a function of the surface tension and the pressure difference between liquid and the bubble interior, with minor contributions from liquid density and viscosity.[55] According to the Rayleigh-Plesset equation, the increase of the internal pressure of the bubble corresponds to an increase of bubble size at any time during the cavitation process.[55, 56] Hence, the extra vapor pressure originated by H_2O_2 decomposition contributes to the formation of a cavitation bubble with larger size, and this increases the probability that NPs are included in the bubble instead of travelling in the liquid phase on bubble front. Inside the bubble, the concentration of solution species is lower and there is a lower chance that iron oxidation occurs, thus AuFe alloy can form. Since surface oxidation and particle cooling are slower than in liquid, due to the lower C_S in the gas phase, nuclei growth and coalescence is possible for a longer time and this allows the production of NPs larger than in ethanol/N_2. Conversely, NPs located in the liquid phase outside the gas bubble undergo to rapid quenching and limited coalescence, and their final size will be smaller.

Since we observed lower surface oxidation than in ethanol/H_2O and water/H_2O_2 samples, it is likely that NPs of the ethanol/H_2O_2 sample are relatively cold when they reach the liquid phase, so that only surface passivation with a protective effect on the inner metal phase occur.

One can not exclude also that the oxidising efficacy of H_2O_2 is diminished by thermal decomposition.[54] In any case, the overall low concentration of oxidising species is favourable for the formation of alloy NPs during LASiS.

Physical Chemistry Chemical Physics Accepted Manuscript

2) Ethanol/N_2 (Figure 7c). In this case, the cavitation bubble has "ordinary" size and growth dynamics, because the extra vapor pressure due to thermal decomposition of H_2O_2 is not present in ethanol/N_2. Therefore, it is likely that NPs form part inside and part outside the cavitation bubble, similarly to what observed in ref.[50, 51]. Due to the low C_S and cooling rate inside the bubble, larger NPs are formed by coalescence of hot nuclei, with very low chance of iron oxidation. Conversely, in the liquid solution, the cooling rate is more rapid and NPs growth is quenched to lower size than in the gas phase. In addition, it is also possible that the larger concentration of oxidant species in the liquid phase (such as H_2O and residuals O_2 contaminants) produces a faster passivation of NPs surface, which hampers nuclei coalescence and particles growth. This can explain why NPs size is lower than in the ethanol/H_2O_2 sample. The presence of some particles with irregular and corral-like shape is also compatible with the interruption of nuclei coalescence by the rapid quenching and/or passivation in liquid. However, the final size distirbution is lognormal, suggesting that no drastic differences exists between NPs formation inside and outside the cavitation bubble, otherwise a bimodal size distribution would be observed.[23] In fact, the overall low concentration of oxidant species is favourable for the formation of alloy NPs, given the overall fast formation kinetics of LASiS.

3) Ethanol/H_2O (Figure 7d). Fluidodynamic and thermodynamic properties of ethanol with 0.2vol% of H_2O are basically equal to that of pure ethanol,[57] hence the dynamics and size of the cavitation bubble is not different from the ethanol/N_2 solution, and NPs are located both inside and outside the cavitation bubble as in the previous case. However, the concentration of oxidising species during NPs formation is larger than in ethanol/N_2, due to the presence of H_2O molecules, which makes possible the formation of iron oxides and hydroxides.

In case of the ethanol/H_2O_2 solution, where the majority of NPs is supposed to form inside the cavitation bubble and the concentration of oxidant molecules is larger than in ethanol/H_2O solution, no iron oxide shells or nanocrescents were observed. Since in ethanol/H_2O sample, iron oxide nanocrescents and small NPs are found, with bimodal size distribution, we speculate that iron oxidation is especially favoured in the liquid phase. We suppose that the growth of NPs outside the cavitation bubble is rapidly interrupted at sizes as small as few nm by the formation of iron oxide and hydroxides on their surface.[24, 28, 32] The formation of iron oxides and hydroxides is more likely here than in ethanol/N_2, where H_2O can be present only as trace impurity.

Besides, experimental evidences suggest that AuFe alloy NPs obtained in ethanol/H_2O have iron content similar to NPs in ethanol/N_2 and ethanol/H_2O_2. This supports the hypothesis that alloy nuclei form in the first instants of LASiS in all cases, namely before the formation of a cavitation

Physical Chemistry Chemical Physics Accepted Manuscript

bubble, when T, p and C_M are high while C_S is low (and oxidant concentration in C_S is lower than in water).

Regarding the fraction of larger NPs which are supposed to form prevalently inside the cavitation bubble, they arrive in the liquid phase with internal temperature and atomic mobility high enough to react with water molecules. In this case, the asymmetric structure of the iron oxide crescent, observed by TEM, may be the trace of the translational dynamics of NPs from the ablation site to the surrounding liquid phase, or just the imprint of C_S gradient. The iron oxide crescent do not form in ethanol/N_2 because there are no H_2O molecules. In ethanol/H_2O_2 the iron oxide crescent is not observed likely because the cavitation bubble is larger and NPs spend more time in the gas phase before encountering the liquid, hence nanoallys have time to cool down before meeting the oxidant molecules in solution.

The occurrence of two NPs formation regimes (i.e. inside and outside the cavitation bubble) are evidenced by the bimodal NPs size distribution.

4) Water/H_2O_2 (Figure 7e). This is the sample obtained in the most oxidising conditions, in fact NPs show a thick iron oxide shell embedding metal NPs with the lowest content of iron among all the samples. Thermal decomposition of H_2O_2 can sustain cavitation bubble growth and expansion, as in the ethanol/H_2O_2 solution. However, water has larger surface tension, heat capacity, vapour pressure, density and viscosity than ethanol, hence the size of the cavitation bubble is lower than in ethanol/H_2O_2 at parity of laser pulse energy. In any case, the density of oxidant molecules inside the cavitation bubble and before bubble formation is the largest of all the four cases considered, and the chance of reaction with iron already in the first ns after laser ablation is very high.

NPs outside cavitation bubble readily react with H_2O and H_2O_2 molecules, forming a network of iron oxide and hydroxide which block particles growth to a size of only 2-4 nm. Larger NPs, which form inside the cavitation bubble, have the chance to interact with solvent species in the subsequent stage of formation, when atomic mobility is large enough to form the thick iron oxide shell around the iron-poor metal core. The final size distribution is bimodal due to the different growth mechanisms of NPs inside and outside the cavitation bubble.

Physical Chemistry Chemical Physics Accepted Manuscript

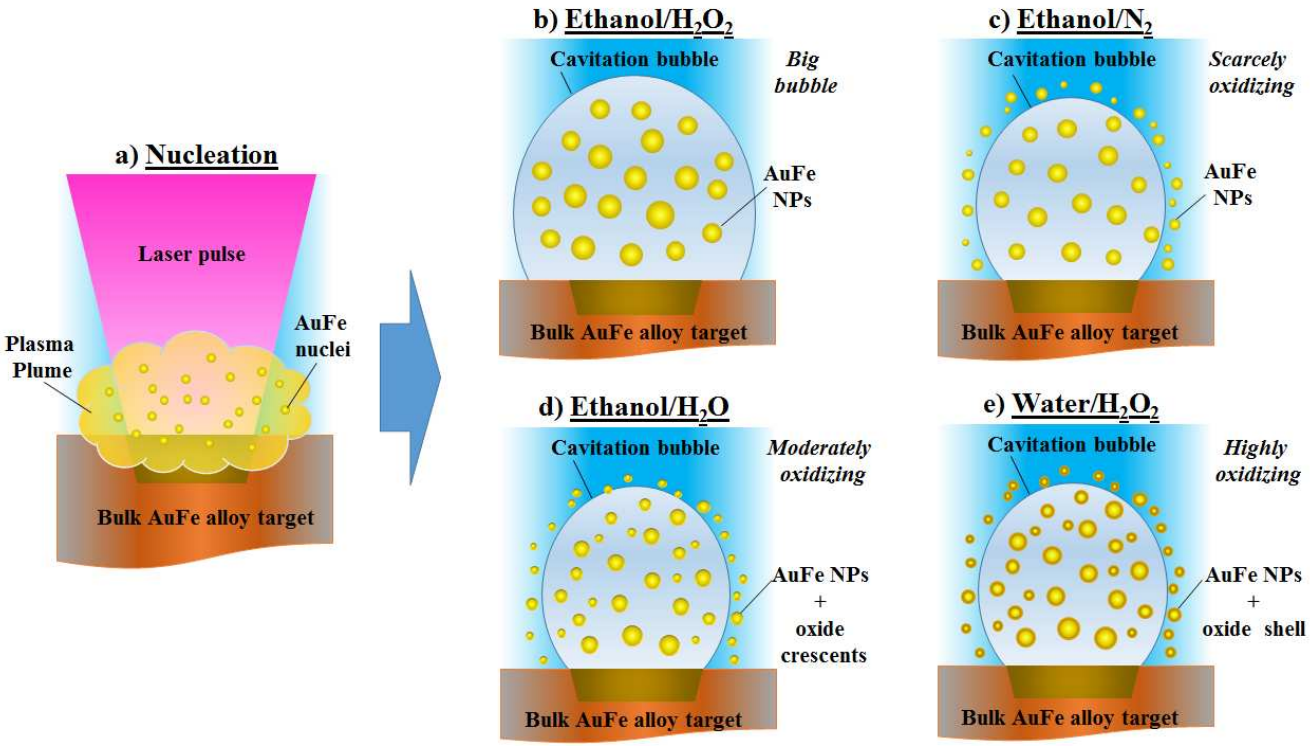

Figure 7. After target ablation and nucleation (a), NPs formation prosecute in different ways depending on the chemical environment selected for LASiS of the nanoalloys: b) NPs in ethanol/H_2O_2 forms prevalently inside the cavitation bubble, which is larger than in the other samples, with scarce probability of iron oxidation, yielding the largest NPs among the four samples and monomodal size distribution. c) NPs in ethanol/N_2 forms both inside and outside the cavitation bubble, with scarce probability of iron oxidation, yielding smaller NPs than in the previous case and monomodal size distribution. d) NPs in ethanol/H_2O forms both inside and outside the cavitation bubble, with moderate probability of iron oxidation, especially in the later stage of NPs formation, yielding smaller NPs than in the previous cases, nanocrescent structures and bimodal size distribution. e) NPs in water/H_2O_2 forms both inside and outside the cavitation bubble, with large probability of iron oxidation, yielding the smallest NPs among all samples, metal@iron-oxide nanoshell structures and bimodal size distribution.

Our experiments showed also that NPs productivity is remarkably larger in case of the ethanol/H_2O solution. In LASiS, productivity is connected to two factors:[23, 25] i) the efficiency of energy transfer from laser pulses to the bulk target, and ii) the effective confinement of the plasma plume on the target by the liquid solution, which is responsible for plasma ablation of the target. The first factor depends on the transparency of the solution at the laser wavelength of 1064 nm. All ethanol solutions have the same absorbance at 1064 nm, however during LASiS the NPs may add a scattering contribution in the near infrared which can decrease significantly the fraction of laser energy delivered to the target. In case of ethanol/H_2O we obtained the smallest NPs, therefore it is possible that their scattering contribution was negligible. This hypothesis is in part supported by the generally larger yield of NPs in water solutions, since we observed lower scattering as a

Physical Chemistry Chemical Physics Accepted Manuscript

consequence of the larger stability and minimial aggregation of NPs synthesized in water compared to ethanol, with the sole exception of the ethanol/H_2O sample.

The plasma confinement on the target depends on the fluidodynamic properties of the liquid solution, such as density, surface tension and viscosity.[23, 25] However, these properties are nearly the same for all ethanol solutions, included the ethanol/H_2O sample, and can not justify the remarkable difference in productivity observed only in one case. Instead, the larger surface tension, density and viscosity of water compared to ethanol are also compatible with a more efficient plasma confinement and the consequently larger productivity reported in Figure 5, with the sole exception of the ethanol/H_2O solution.

Conclusions.

In summary, we investigated the effect of chemical environment on structure and composition of metastable nanoalloys generated by laser ablation in liquid solution. In our experiments we investigated different synthetic conditions for LASiS, such as the use of water instead of ethanol, the bubbling of inert gases and the addition of few vol% of H_2O_2 and H_2O. The importance of chemical interactions between solution species and ablated materials was demonstrated by the fact that, by changing the composition of the solution, different nanostructures were obtained such as metallic nanoalloys, metal nanoparticles coated by oxide nanocrescents or metal@oxide nanoshells. The results are interpreted with the interaction of the ablated material with solvent molecules and with oxidising compounds with concentration above 0.1vol%. We also evidenced a negligible effect from atmospheric gases on the products. Conversely, solution decomposition is important for the rise of the cavitation bubble, which affects the coalescence and growth of nanoparticles. In particular, a crucial role is played by the distribution of NPs inside or outside the cavitation bubble which is generated by laser pulses, especially when target species react with solution species. This is reflected in the final stoichiometry, in the structure and in the size distribution of nanoalloys.

The results give important information for the realization of metastable nanoalloys by LASiS, and in particular suggest that the size and lifetime of the cavitation bubble should be increased as much as possible to preserve the alloy composition, in addition to the obvious consideration that the concentration of reactive species which can interfere with the alloy stoichiometry should be reduced at minimum.

These results expand the knowledge about the mechanism of formation of nanoalloys by LASiS, and show how to obtain multielement nanoparticles of huge interest for nanomedicine, plasmonics, magneto-plasmonics and catalysis.

Physical Chemistry Chemical Physics Accepted Manuscript

Acknowledgments.

Financial support from University of Padova (PRAT no. CPDA114097/11 and Progetto Strategico STPD11RYPT_001) and MIUR (PRIN MULTINANOITA no. 2010JMAZML_001) is gratefully acknowledged.

References

1 A. Villa, D. Wang, D. S. Su and L. Prati, *Catal. Sci. Technol.*, 2015, **5,** 55-68.

2 J. Kaiser, L. Leppert, H. Welz, F. Polzer, S. Wunder, N. Wanderka, M. Albrecht, T. Lunkenbein, J. Breu and S. Kümmel, *Physical Chemistry Chemical Physics*, 2012, **14,** 6487-6495.

3 F. J. Ibañez and F. P. Zamborini, *ACS Nano*, 2008, **2,** 1543-1552.

4 M. H. Tang, C. Hahn, A. J. Klobuchar, J. W. D. Ng, J. Wellendorff, T. Bligaard and T. F. Jaramillo, *Phys. Chem. Chem. Phys.*, 2014, **16,** 19250-19257.

5 M. Branca, F. Pelletier, B. Cottin, D. Ciuculescu, C. Lin, R. Serra, J. Mattei, M. Casanove, R. Tan and M. Respaud, *Faraday Discuss.*, 2014, .

6 S. Costacurta, L. Malfatti, P. Innocenzi, H. Amenitsch, A. Masili, A. Corrias and M. F. Casula, *Microp. Mesop. Mater.*, 2008, **115,** 338-344.

7 V. Amendola, S. Scaramuzza, L. Litti, M. Meneghetti, G. Zuccolotto, A. Rosato, E. Nicolato, P. Marzola, G. Fracasso and C. Anselmi, *Small*, 2014, **10,** 2476-2486.

8 R. Ferrando, J. Jellinek and R. L. Johnston, *Chem. Rev.*, 2008, **108,** 845-910.

9 G. Barcaro, L. Sementa and A. Fortunelli, *Phys. Chem. Chem. Phys.*, 2014, **16,** 24256-24265.

10 M. Cerbelaud, R. Ferrando, G. Barcaro and A. Fortunelli, *Phys. Chem. Chem. Phys.*, 2011, **13,** 10232-10240.

11 R. Ismail and R. L. Johnston, *Phys. Chem. Chem. Phys.*, 2010, **12,** 8607-8619.

12 I. V. Yudanov and K. M. Neyman, *Phys. Chem. Chem. Phys.*, 2010, **12,** 5094-5100.

13 R. L. Johnston and J. P. Wilcoxon, *Metal Nanoparticles and Nanoalloys*, Elsevier, 2012.

14 N. E. Kolli, L. Delannoy and C. Louis, *J. Catal.*, 2013, **297,** 79-92.

15 C. Tojo, M. de Dios, D. Buceta and M. López-Quintela, *Phys. Chem. Chem. Phys.*, 2014, **16,** 19720-19731.

16 N. Tabrizi, Q. Xu, N. van der Pers and A. Schmidt-Ott, *J. Nanop. Res.*, 2010, **12,** 247-259.

17 P. Mukherjee, P. Manchanda, P. Kumar, L. Zhou, M. J. Kramer, A. Kashyap, R. Skomski, D. Sellmyer and J. E. Shield, *ACS Nano*, 2014, **8,** 8113-8120.

18 H. Nabika, K. Akamatsu, M. Mizuhata, A. Kajinami and S. Deki, *J. Mater. Chem*, 2002, **12,** 2408-2411.

Physical Chemistry Chemical Physics Accepted Manuscript

19 Z. Jiao, M. Sivayoganathan, W. W. Duley, P. He and Y. N. Zhou, *J. Phys. Chem. C*, 2014, **118,** 24746-24751.

20 Z. Zhang, Y. Wang and X. Wang, *Nanoscale*, 2011, **3,** 1663-1674.

21 R. P. Doherty, J. Krafft, C. Méthivier, S. Casale, H. Remita, C. Louis and C. Thomas, *J. Catal.*, 2012, **287,** 102-113.

22 L. Lee, C. Xiao, W. Huang and Y. Zhao, *New J. Chem.*, 2015, .

23 V. Amendola and M. Meneghetti, *Phys. Chem. Chem. Phys.*, 2013, **15,** 3027-3046.

24 V. Amendola, M. Meneghetti, O. M. Bakr, P. Riello, S. Polizzi, D. H. Anjum, S. Fiameni, P. Arosio, T. Orlando and C. de Julian Fernandez, *Nanoscale*, 2013, **5,** 5611-5619.

25 V. Amendola and M. Meneghetti, *Phys. Chem. Chem. Phys.*, 2009, **11,** 3805-3821.

26 J. Jakobi, S. Petersen, A. Menéndez-Manjón, P. Wagener and S. Barcikowski, *Langmuir*, 2010, **26,** 6892-6897.

27 K. D. Malviya and K. Chattopadhyay, *J. Phys. Chem. C*, 2014, **118,** 13228-13237.

28 V. Amendola, S. Scaramuzza, S. Agnoli, S. Polizzi and M. Meneghetti, *Nanoscale*, 2014, **6,** 1423-1433.

29 N. Mottaghi, M. Ranjbar, H. Farrokhpour, M. Khoshouei, A. Khoshouei, P. Kameli, H. Salamati, M. Tabrizchi and M. Jalilian-Nosrati, *Appl. Surf. Sci.*, 2014, **292,** 892-897.

30 E. Gordon, A. Karabulin, V. Matyushenko, V. Sizov and I. Khodos, *Phys. Chem. Chem. Phys.*, 2014, **16,** 25229-25233.

31 H. Okamoto, T. Massalski, L. Swartzendruber and P. Beck, *Journal of Phase Equilibria*, 1984, **5,** 592-601.

32 V. Amendola, P. Riello, S. Polizzi, S. Fiameni, C. Innocenti, C. Sangregorio and M. Meneghetti, *J. Mater. Chem.*, 2011, **21,** 18665-18673.

33 J. Yeh and I. Lindau, *Atomic Data and Nuclear Data Tables*, 1985, **32,** 1-155.

34 S. Tanuma, C. J. Powell and D. R. Penn, *Surf. Interface Anal.*, 1993, **20,** 77-89.

35 U. Kreibig and M. Vollmer, *Optical Properties of Metal Clusters*, Springer, Berlin, 1995.

36 V. Amendola and M. Meneghetti, *J. Phys. Chem. C*, 2009, **113,** 4277-4285.

37 J. Santillán, L. Scaffardi and D. Schinca, *J. Phys. D*, 2011, **44,** 105104.

38 J. Santillán, F. Videla, M. F. van Raap, D. Schinca and L. Scaffardi, *J. Appl. Phys.*, 2013, **113,** 134305.

39 Y. Lee, Y. Kudryavtsev, V. Nemoshkalenko, R. Gontarz and J. Rhee, *Phys. Rev. B*, 2003, **67,** 104424.

40 E. D. Palik, *Handbook of Optical Constants of Solids*, Academic Press, 1985.

41 V. Amendola, O. M. Bakr and F. Stellacci, *Plasmonics*, 2010, **5,** 85-97.

Physical Chemistry Chemical Physics Accepted Manuscript

42 V. Amendola, M. Meneghetti, G. Granozzi, S. Agnoli, S. Polizzi, P. Riello, A. Boscaini, C. Anselmi, G. Fracasso and M. Colombatti, *J. Mater. Chem.*, 2011, **21,** 3803-3813.

43 J. Tokunaga, *J. Chem. Eng. Data*, 1975, **20,** 41-46.

44 P. Luehring and A. Schumpe, *J. Chem. Eng. Data*, 1989, **34,** 250-252.

45 R. Battino and H. L. Clever, *Chem. Rev.*, 1966, **66,** 395-463.

46 T. Schnabel, J. Vrabec and H. Hasse, *Fluid Phase Equilib.*, 2005, **233,** 134-143.

47 A. Ben-Naim, *J. Phys. Chem.*, 1967, **71,** 4002-4007.

48 J. Sylvestre, S. Poulin, A. V. Kabashin, E. Sacher, M. Meunier and J. H. Luong, *J. Phys. Chem. B*, 2004, **108,** 16864-16869.

49 Y. Li and T. Tsui, *J. Geophys. Res.*, 1971, **76,** 4203-4207.

50 S. Ibrahimkutty, P. Wagener, A. Menzel, A. Plech and S. Barcikowski, *Appl. Phys. Lett.*, 2012, **101,** 103104.

51 P. Wagener, S. Ibrahimkutty, A. Menzel, A. Plech and S. Barcikowski, *Phys.Chem.Chem.Phys.*, 2013, **15,** 3068-3074.

52 L. Wang, T. L. Tan and D. D. Johnson, *Nano Lett.*, 2014, **14,** 7077-7084.

53 E. Panizon, D. Bochicchio, G. Rossi and R. Ferrando, *Chem. Mater.*, 2014, **26,** 3354-3356.

54 P. A. Giguère and I. Liu, *Canad. J. Chem.*, 1957, **35,** 283-293.

55 M. S. Plesset and A. Prosperetti, *Annu. Rev. Fluid Mech.*, 1977, **9,** 145-185.

56 K. Sasaki, T. Nakano, W. Soliman and N. Takada, *Appl. Phys. Expr.*, 2009, **2,** 046501.

57 G. Vazquez, E. Alvarez and J. M. Navaza, *J. Chem. Eng. Data*, 1995, **40,** 611-614.

Physical Chemistry Chemical Physics Accepted Manuscript

TOC Text and Graph

Metastable nanoalloys, metal-oxide nanocrescents and metal@oxide nanoshells are generated by laser ablation in liquid solution (LASiS)

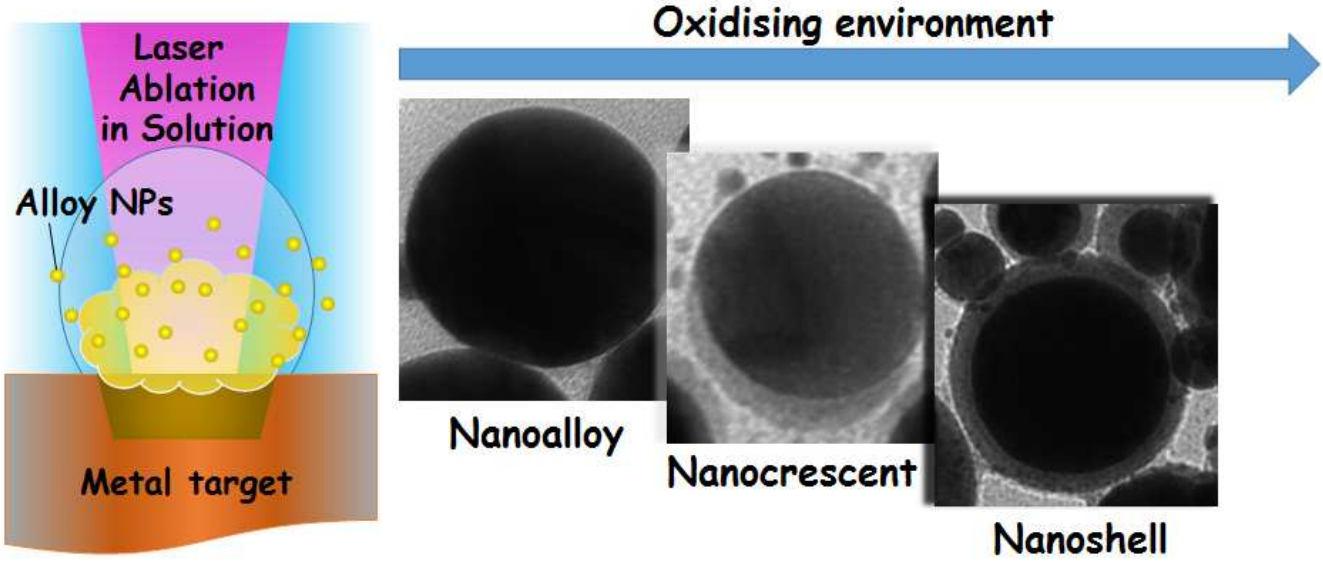

Physical Chemistry Chemical Physics Accepted Manuscript